Journal of Zhejiang University-SCIENCE A (Applied Physics & Engineering)
ISSN 1673-565X (Print); ISSN 1862-1775 (Online)
www.zju.edu.cn/jzus; www.springerlink.com
E-mail: jzus@zju.edu.cn

A new method for studying the 3D transient flow of misaligned journal bearings in flexible rotor-bearing systems*

Qiang LI[†1], Shu-lian LIU[2], Xiao-hong PAN[3], Shui-ying ZHENG[†‡1]

([1]*Institute of Chemical Machinery, Zhejiang University, Hangzhou 310027, China*)

([2]*Department of Electro-Mechanical Engineering, Zhejiang University of Science and Technology, Hangzhou 310023, China*)

([3]*Institute of Modern Manufacture Engineering, Zhejiang University, Hangzhou 310027, China*)

[†]E-mail: liqiangsydx@163.com; zhengshuiying@zju.edu.cn

Received Oct. 19, 2011; Revision accepted Dec. 29, 2011; Crosschecked Feb. 27, 2012

Abstract: The effects of journal misalignment on the transient flow of a finite grooved journal bearing are presented in this study. A new 3D computational fluid dynamics (CFD) analysis method is applied. Also, the quasi-coupling calculation of transient fluid dynamics of oil film in journal bearing and rotor dynamics is considered in the analysis. Based on the structured mesh, a new approach for mesh movement is proposed to update the mesh volume when the journal moves during the fluid dynamics simulation of an oil film. Existing dynamic mesh models provided by FLUENT are not suitable for the transient oil flow in journal bearings. The movement of the journal is obtained by solving the moving equations of the rotor-bearing system with the calculated film pressure as the boundary condition of the load. The data exchange between fluid dynamics and rotor dynamics is realized by data files. Results obtained from the CFD model were consistent with previous experimental results on misaligned journal bearings. Film pressure, oil film force, friction torque, misalignment moment and attitude angle were calculated and compared for misaligned and aligned journal bearings. The results indicate that bearing performances are greatly affected by misalignment which is caused by unbalanced excitation, and the CFD method based on the fluid-structure interaction (FSI) technique can effectively predict the transient flow field of a misaligned journal bearing in a rotor-bearing system.

Key words: Misalignment, Transient flow, Computational fluid dynamics (CFD), Fluid-structure interaction (FSI), Journal bearing

doi:10.1631/jzus.A1100228 **Document code:** A **CLC number:** TH113.31

1 Introduction

Journal bearings have been widely used in rotating machinery. Due to manufacturing errors leading to deflection of the shaft, bearing housing supports and other parts of the rotor-bearing system, journal bearings normally operate in a misaligned condition. Generally, misalignment has a considerable effect on the lubrication performance of a journal bearing, through its effects on pressure distribution, load carrying capacity and fluid film thickness, etc. Hence, misalignment is predicted to influence significantly the dynamic characteristics, vibration behavior and stability of a rotor-bearing system. Therefore, it is important to investigate the effects of misalignment on the lubrication of journal bearings.

McKee and McKee (1932) first analyzed the effects of misalignment on pressure distribution in the axial direction of a journal bearing. Dubois *et al*. (1951; 1955; 1957) experimentally investigated the pressure field and the misalignment of couples under journal misalignment. Smalley and McCallion (1966) gave a thorough discussion of bearing misalignment

---

‡ Corresponding author

* Project supported by the National High-Tech R&D (863) Program of China (No. 2009AA04Z413), and the Natural Science Foundation of Zhejiang Province (No. Y1110109), China

for ungrooved bearings with slenderness ratios of 0.5 and 0.75. Asanable *et al*. (1971) investigated the minimum film thickness and friction force of a two-groove bearing under misalignment only in the vertical plane. Pinkus and Bupara (1979) presented a comprehensive analysis of misaligned bearings and charts which revealed some of the salient features of different misaligned journal bearings. Mokhtar *et al*. (1985) presented an adiabatic solution for a misaligned journal bearing with axial feeding. Buckholz and Lin (1986) analyzed the effects of misalignment on the load and cavitation of journal bearings with non-Newtonian lubricants. Jiang and Chang (1987) presented an adiabatic solution for a misaligned journal bearing with non-Newtonian lubricants obeying the power-law fluid model. Vijayaraghavan and Keith (1989; 1990) studied the effects of misalignment on the performance of a line-grooved journal bearing for both flooded and starved inlet conditions using a modified Elrod cavitation algorithm. Bou-Said and Nicolas (1992) presented the influence of the misalignment of geometrical parameters on the static and dynamic characteristics of hybrid bearings in laminar and turbulent flow regimes, and compared experimental results with results obtained from two numerical procedures. Qiu and Tieu (1995; 1996) attempted a theoretical and experimental investigation on the characteristics of two misaligned journal bearings. All static and dynamic characteristics of the grooved journal bearing under different eccentricity and misalignment conditions were presented and compared with experimental data. Arumugam *et al*. (1997) presented an algorithm for identification of stiffness and damping coefficients of a misaligned three-lobe bearing. Banwait *et al*. (1998) observed the thermohydrodynamic (THD) effects in misaligned circular plain journal bearings. Guha (2000) incorporated the effects of isotropic roughness, eccentricity ratio and degree of misalignment in the analysis of the steady-state performance characteristics of a misaligned journal bearing. Bouyer and Fillon (2002) experimentally analyzed misalignment effects on performance with a plain journal bearing of 100 mm diameter. Pierre *et al*. (2004) developed a 3D THD model of misaligned plain journal bearings considering thermal and cavitation effects. Boedo and Booker (2004) investigated the transient and steady-state behavior of grooveless misaligned bearings. Ma (2008) incorporated the effects of couple stress and elasticity of the liner in the analysis of the performance characteristics of a dynamically loaded journal bearing. Sun *et al*. (2010) calculated the lubrication characteristics of a misaligned journal bearing considering the viscosity-pressure relationship of the oil, the surface roughness, the deformation of the bearing surface and thermal effects. Jiang and Khonsari (2010) investigated the influence of misalignment on a journal bearing using a 3D THD model with the shaft temperature field. They used a mass-conserving cavitation algorithm in their analysis. However, the above lubrication analyses of misaligned journal bearings were conducted under some specified preconditions and did not consider the interaction between the shaft and the bearing, except for the theoretical and experimental work in the steady-state condition by Sun and Gui (2004) and Sun (2005; 2007). In the present work, the influence of misalignment on the transient flow field of a journal bearing considering fluid-structure interactions (FSIs) in a flexible rotor-bearing system was investigated.

From the literature review, it is apparent that the effects of misalignment on the performance of journal bearings have been analysed using a generalized Reynolds equation, which is simplified from the Navier-Stokes equations and the equation of continuity. These solutions of the Reynolds equation may need more work to meet requirements when a complex flow geometry is used or when a more detailed analysis is necessary. In these situations, general computational fluid dynamics (CFD) techniques, which use the full Navier-Stokes equations and provide precise solutions to the governing flow equation without many of the simplifying assumptions, would be very beneficial for analysis of the fluid field in a journal bearing.

Due to the rapid development of computer technology, there have been many recent studies on the lubrication analysis of journal bearings using CFD techniques. Chen *et al*. (1998) showed how CFD can be used advantageously to solve steady-state hydrodynamic lubrication problems pertaining to slider bearings, step bearings, journal bearings and squeeze-film dampers. The same method was applied to a circular orbiting squeeze film damper with a central circumferential feed groove to study the influence of end seal clearance and flow path length (Chen *et al.*, 2000). Guo *et al.* (2005) developed a CFD approach, using CFX-TASC flow software, to simulate the pressure field and calculate the static and dynamic characteristics of various fixed geometry bearings and squeeze film dampers. Gertzos *et al.* (2008) examined performance characteristics and core formation in a journal bearing lubricated with a Bingham fluid and a Newtonian lubricant by means of CFD analysis. The available dynamic mesh technique and half-Sommerfeld boundary condition were used in their study. Meruane and Pascual (2008) proposed the numerical identification of nonlinear fluid film bearing parameters from a large journal orbit considering a CFD model of a plain journal bearing under transient conditions with FSI. Liu *et al.* (2010) developed a methodology combining CFD and FSI to investigate the effects of the elastic deformation of a rotor and bearing using ADINA. However, a CFD-FSI methodology has never been used to analyze the transient flow field of a misaligned grooved journal bearing in a rotor-bearing system.

Cavitation is the disruption of what would otherwise be a continuous liquid phase by the presence of a gas or vapor or both (Dowson *et al.*, 1979). The occurrence of cavitation in a journal bearing is largely undesirable due to its negative effects that reduce the load capacity, power, friction coefficient and bearing torque (Jakobsson *et al.*, 1957). Therefore, it is important to establish a boundary condition which can precisely describe the transition between the liquid and vapor phases. Classical boundary conditions violate the principle of conservation of mass and cannot correctly represent the flow physics (Vijayaraghavan *et al.*, 1989; 1990). Therefore, in this paper the mass conserving boundary condition that can appropriately describe the fluid film rupture and reformation is used to model cavitation in the fluid domain.

In the present work, a 3D simulation model of a journal bearing under the misalignment condition is developed using the CFD software FLUENT. The results of a CFD model are compared with the experimental work of Tieu and Qiu (1996) and found to be in good agreement. To make the lubrication analysis close to the actual situation and applicable to the design of rotor-bearing systems, the main focus of this paper is to direct CFD predictions with FSI at the transient flow field, for a realistic misaligned two-axial grooved bearing in a flexible rotor-bearing system. In practice, due to the magnitude of the difference between the clearance and the dimensions of the journal bearing, the use of unstructured grids and dynamic mesh models in FLUENT will stop the calculation process due to numerical failure or the negative volume of grids in the transient condition. Therefore, a new mesh moving method based on the structured grids and applied to the transient analysis of a misaligned journal bearing, is proposed in this paper. The advantage of this mesh movement approach is that it can generate high structured grid quality under large journal orbital motion. Based on this mesh movement method, the quasi-coupling calculation of the transient fluid dynamics of the oil film in a journal bearing and rotor dynamics is developed and used to analyze the effects of misalignment on the transient flow field and performance characteristics of a journal bearing. The results of this work provide a basis for studying the nonlinear dynamic behavior of a realistic rotor-bearing system.

2 Theory of the model

2.1 Equations governing fluid dynamics

In this study, the fluid flow is described by the integral form of the conservation laws for mass and momentum in an arbitrary volume V bounded by a moving boundary dV as

$$\begin{aligned}&\frac{\mathrm{d}}{\mathrm{d}t}\int_V \rho_{\mathrm{m}}\phi \mathrm{d}V + \int_{\partial V}\rho_{\mathrm{m}}\phi(\boldsymbol{u}_{\mathrm{m}}-\boldsymbol{u}_{\mathrm{g}})\mathrm{d}\boldsymbol{A}\\ &\quad=\int_{\partial V}\Gamma\nabla^2\phi\mathrm{d}\boldsymbol{A}+\int_V S_\phi \mathrm{d}V,\end{aligned} \tag{1}$$

where ρ_{m} is the mixture density when considering cavitation, $\boldsymbol{u}_{\mathrm{m}}$ is the velocity vector of mixture, $\boldsymbol{u}_{\mathrm{g}}$ is the boundary velocity of the moving mesh, $\boldsymbol{A}$ is the area vector of the control volume. The universal variable ϕ, the diffusion coefficient Γ, and the generalized source term S_ϕ are given by

$$\phi=\begin{bmatrix}1\\u_j\end{bmatrix},\ \Gamma=\begin{bmatrix}0\\\mu_{\mathrm{m}}\end{bmatrix},\ S_\phi=\begin{bmatrix}0\\-\mathrm{grad}\,p\end{bmatrix}, \tag{2}$$

where u_j is the jth component of velocity, μ_m is the viscosity of mixture, and p is the lubricant pressure.

Besides the conservation equations above, the equation of state between the fluid density and pressure is required for closure of the momentum and continuity equations.

2.2 Cavitation model

As mentioned above, the fluid film of a journal bearing may rupture due to heavy external load or high operating rotational speed. To take account of this, the mass conserving boundary condition which is based on the so-called "full cavitation model" (Singhal *et al.*, 2002) in FLUENT was used in this study. The cavitation model is built on a framework of multi-phase flows and accounts for all first-order effects.

The governing equations are modified by taking into consideration of the effects of the change in void fraction on ρ_m and μ_m. The "full cavitation model" can handle the large density changes associated with the fluid phase change without requiring a prior determination of the location, extent, or type of cavitation.

The fluid density, as a function of the mass fraction of gas f_g and vapor f_v, which is computed by solving a transport equation coupled with the mass and momentum conservation equations, can be represented by

$$\frac{1}{\rho_m}=\frac{f_v}{\rho_v}+\frac{f_g}{\rho_g}\frac{1-f_v-f_g}{\rho_l}, \tag{3}$$

where ρ_v, ρ_g, and ρ_l are densities of vapor, gas and liquid, respectively, and the volume fractions of gas α_g and vapor α_v can be written as

$$\alpha_g=f_g\frac{\rho_m}{\rho_g},\ \ \alpha_v=f_v\frac{\rho_m}{\rho_v}. \tag{4}$$

The total gas-mass fraction (f=f_v+f_g) is governed by the following transport equation:

$$\frac{\partial}{\partial t}(\rho_m f)+\nabla(\rho_m \boldsymbol{u}_m f)=\nabla(\mu_m \nabla f)+R_e-R_c, \tag{5}$$

where the source terms R_e and R_c denote vapor generation and condensation rate, respectively, and can be functions of flow parameters and fluid properties:

$$R_e=C_e\frac{V_{ch}}{\sigma}\rho_l\rho_v\sqrt{\frac{2(p_{sat}-p)}{3\rho_l}}(1-f_v-f_g),\quad p<p_{sat}, \tag{6}$$

$$R_c=C_c\frac{V_{ch}}{\sigma}\rho_l\rho_v\sqrt{\frac{2(p-p_{sat})}{3\rho_l}}f_v,\ p>p_{sat}, \tag{7}$$

where V_{ch} is a characteristic velocity, σ is the surface tension coefficient of the liquid, p_{sat} is the liquid saturation vapor pressure at the given temperature, C_e and C_c are empirical constants with recommended values of C_e=0.02 and C_c=0.01, respectively, which have been calibrated using experimental data covering a very wide range of flow conditions, and do not require adjustment for different problems.

2.3 Modeling of rotor-bearing systems

For a flexible rotor-bearing system, the system motion equations can be given as follows (Zheng *et al.*, 1993; 2005):

$$\boldsymbol{M}\ddot{\boldsymbol{X}}+\boldsymbol{C}\dot{\boldsymbol{X}}+\boldsymbol{K}\boldsymbol{X}=\boldsymbol{B}_1\boldsymbol{F}_u+\boldsymbol{B}_2\boldsymbol{G}+\boldsymbol{B}_3\boldsymbol{F}+\boldsymbol{B}_3'\boldsymbol{M}_m, \tag{8}$$

where $\boldsymbol{X}$ is the general coordinate of system, $\boldsymbol{M}$, $\boldsymbol{C}$, and $\boldsymbol{K}$ are mass, damping and stiffness matrices, respectively, $\boldsymbol{B}_i$ (i=1,2,3) is the location matrix of forces, and $\boldsymbol{B}_3'$ is the location matrix of the misalignment moment, $\boldsymbol{F}_u$ is the unbalanced force due to mass eccentricity, $\boldsymbol{G}$ is the gravity of rotor supported by bearing, $\boldsymbol{F}$ is the oil film force of the journal bearing, and $\boldsymbol{M}_m$ is the misalignment moment. To fully describe the rotor motion and simplify the calculation, the three-order polynomial is selected as the location function.

Considering the change in the shaft diameter and the existence of additional mass, the shaft in this study is divided into 37 portions, i.e., there are 37 location functions in the x and y directions.

2.4 Performance characteristics

Bearing performance calculations can be carried out during the transient analysis of a misaligned journal bearing in a rotor-bearing system with a known pressure field. The nonlinear oil film force components in x and y coordinates are found from

$$F_x = R\int_0^L \int_0^{2\pi} p\sin\theta \mathrm{d}\theta \mathrm{d}z, \tag{9}$$

$$F_y = R\int_0^L \int_0^{2\pi} p\cos\theta \mathrm{d}\theta \mathrm{d}z, \tag{10}$$

where R is the bearing radius, L is the bearing width, and θ is the circumferential coordinate. The total oil film force F is

$$F = \sqrt{F_x^2 + F_y^2}. \tag{11}$$

In addition to the force components, two components of the misalignment moment in x and y coordinates can be obtained:

$$M_x = R\int_0^L \int_0^{2\pi} pz\cos\theta \mathrm{d}\theta \mathrm{d}z, \tag{12}$$

$$M_y = R\int_0^L \int_0^{2\pi} pz\sin\theta \mathrm{d}\theta \mathrm{d}z, \tag{13}$$

and the total misalignment moment can be calculated as

$$M_\mathrm{m} = \sqrt{M_x^2 + M_y^2}. \tag{14}$$

The friction force can be computed by integrating the shear stress over the bearing surface, and the friction torque is obtained from

$$M_\tau = R^2\int_0^L \int_0^{2\pi} \tau \mathrm{d}\theta \mathrm{d}z, \tag{15}$$

where τ is the shear stress.

3 Numerical procedure

3.1 Mesh movement

During the transient analysis of a misaligned journal bearing, if the lubricant fluid domain involves irregular movement of the journal, then FLUENT capable of 3D simulation and mesh movement is used. Due to the difference in magnitude between the clearance and the dimensions of the journal bearing, a minor change in the fluid domain can greatly affect the results. Thus, an appropriate dynamic mesh method is necessary to model flows where the shape of the domain is changing with time due to motion of the journal during the transient run, and the motion of the journal is modeled by solving the rotor dynamics equations.

FLUENT has three types of dynamic mesh methods: the spring smoothing method, the dynamic layering method and the local remeshing method (FLUENT, 2006). But there are some disadvantages of these dynamic mesh methods that make them unsuitable for a transient run. For example, the spring smoothing method is used for relatively small deformations, and a large deformation will result in a highly skewed element. The dynamic layering algorithm is limited to complex geometry, and the local remeshing algorithm is available only for triangular and tetrahedral elements.

Transient simulations are highly dependent on grid quality. Using unstructured grids and dynamic mesh models in FLUENT as mentioned above will stop the calculation process due to numerical failure or the negative volume of grids (Ngondi *et al.*, 2010). Therefore, a new mesh moving method based on a structured grid applied to FLUENT is proposed in this study.

Fig. 1 shows a cross-section of a simplified plain journal bearing at any axial position. To describe the methodology of mesh movement clearly, the journal bearing structure shown has a larger clearance than in reality. J' represents the current eccentricity position after the journal moves from the upper position marked J, and the movement distance is defined by $\boldsymbol{d}$ $(x_d, y_d, 0)$ in Cartesian coordinates. P denotes an arbitrary point in the clearance of the journal bearing and is assumed to project along a mesh line that connects one point P_2 on the journal and another P_1 on the static bearing. When the journal is moved by $\boldsymbol{d}$, the new coordinates of P_2 in the journal are defined by

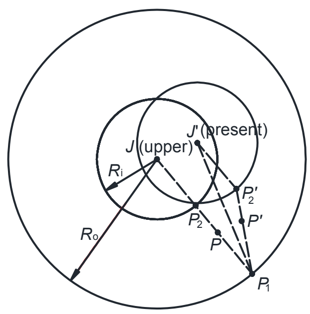

Fig. 1 Annular cavity with moved journal

$$x_{p_2'} = x_{p_2} + x_d,\ y_{p_2'} = y_{p_2} + y_d, \tag{16}$$

where x_{p_2}, y_{p_2} are x and y coordinates of P_2, and $x_{p_2'}$, $y_{p_2'}$ are x and y coordinates of P_2'.

If the displacement distance of the grid in the journal is assumed to be the largest, and the node of the stator surface is assumed to stay still, then between the inner journal and the static bearing, the movement distance of the node decreases from the moved journal to the bearing. Therefore, the new position of P is transformed using

$$x_{p'} = x_p + \frac{N_i}{N} x_d,\ y_{p'} = y_p + \frac{N_i}{N} y_d, \tag{17}$$

where N_i is the number of the radial reticulate layer in which P is located, and N is the total amount of radial reticulate layers in the annular clearance.

Fig. 2 shows an axial section of the journal bearing. K_1' represents the current position of the intermediate node after the journal moves from the upper position marked K_1. The movement distance and axial misaligned angle are defined by $\boldsymbol{s}$ (x_s,y_s,0) and α (α_x, α_y,0) respectively, which are obtained using the rotor dynamics equations and the user-FORTRAN source code interface of FLUENT.

There is an arbitrary point in the fluid domain which is assumed to project along a mesh line that connects one point K'' on the bearing and another point K on the journal. K' denotes the corresponding point in the journal after misalignment. Therefore, the new position of K' is calculated by

$$\begin{cases} x_{K'} = x_s + (z_K - z_{K_1})\tan\alpha_x, \\ y_{K'} = y_s + (z_K - z_{K_1})\tan\alpha_y. \end{cases} \tag{18}$$

For transient simulation, the governing equations must be discretized in both space and time. A first-order implicit time discretization is used as follows:

$$\frac{\mathrm{d}}{\mathrm{d}t}\int_V \rho_{\mathrm{m}}\phi \mathrm{d}V = \frac{(\rho_{\mathrm{m}}\phi V)^{n+1} - (\rho_{\mathrm{m}}\phi V)^n}{\Delta t}, \tag{19}$$

where the superscripts n+1 and n denote the new and old time levels, respectively. Using the dynamic mesh method, the volume V^{n+1} can be expressed as

$$V^{n+1} = V^n + \frac{\mathrm{d}V}{\mathrm{d}t}\Delta t. \tag{20}$$

The described mesh movement algorithm proposed in this study was tested using FLUENT. The update of the mesh volume can be handled automatically by FLUENT at each time step based on the new boundary position.

Fig. 3a shows a cross-section of the journal bearing which is meshed with a structured hexahedral grid. To describe the capabilities of the method clearly, this case models a simplified bearing structure with larger clearance than in reality. Fig. 3b shows that the grids after the inner journal have moved a certain distance. The process is stopped manually without any mesh distortion or numerical failure. A corresponding side view of the journal bearing is shown in Fig. 4.

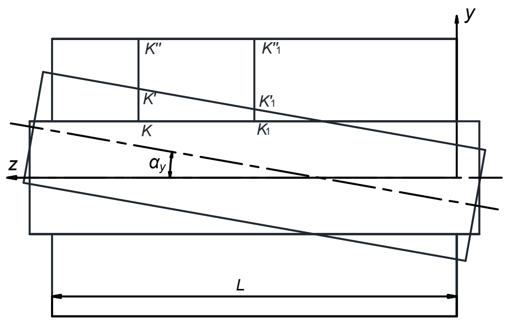

Fig. 2 Axial cavity with moved journal

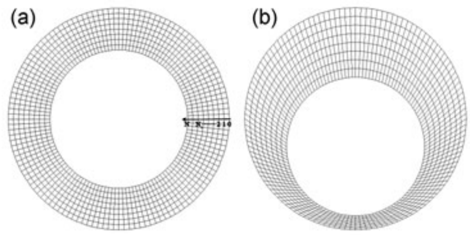

Fig. 3 Front view of the meshed journal bearing
(a) Initial grids; (b) Moved grids

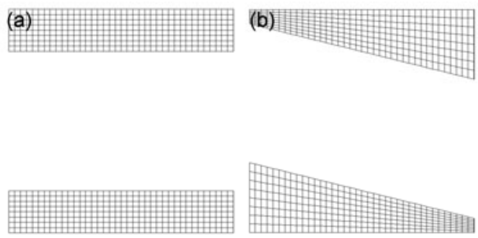

Fig. 4 Side view of the meshed journal bearing
(a) Initial grids; (b) Moved grids

Note that this methodology can keep mesh angles optimal under the combination of large misalignment and eccentricity. Therefore, the proposed mesh movement method is suitable for the transient simulation of a misaligned journal bearing in a rotor-bearing system.

3.2 Fluid-structure interaction

To simulate the transient flow field of a misaligned journal bearing under disturbance in a rotor-bearing system, an FSI method combining FLUENT with FORTRAN is used. Solid dynamic computation in rotor dynamics is quite well developed (Zheng *et al.*, 1993; 2005; Li *et al.*, 2011). Thus, 3D unsteady flow field simulation of the journal bearing under perturbation could be easily solved with the mesh movement method provided. The data exchange between fluid dynamics and rotor dynamics is realized by data files, which makes quasi-coupling calculation between the fluid dynamics of the oil film in a journal bearing and rotor dynamics possible. The FSI is described by the weak coupling method. This means that the solid and fluid equations are computed in every time step, and the data transferred at the solid-fluid interface is used as the boundary condition of the two domains. One worthy point of the weak coupling method is its utmost use of matured CFD software without rewriting the code. The coupling between the CFD method FLUENT and the rotor simulation code FORTRAN is carried out as shown in Fig. 5.

The steady flow field of an aligned journal bearing is first simulated by FLUENT to eliminate the influence of the initial value. After that, the nonlinear oil film force and moment are obtained by integrating the fluid film pressure of the upper iteration step through the application of user-defined function (UDF). With the fluid boundary condition transferred to a data file, the perturbation displacement is obtained by

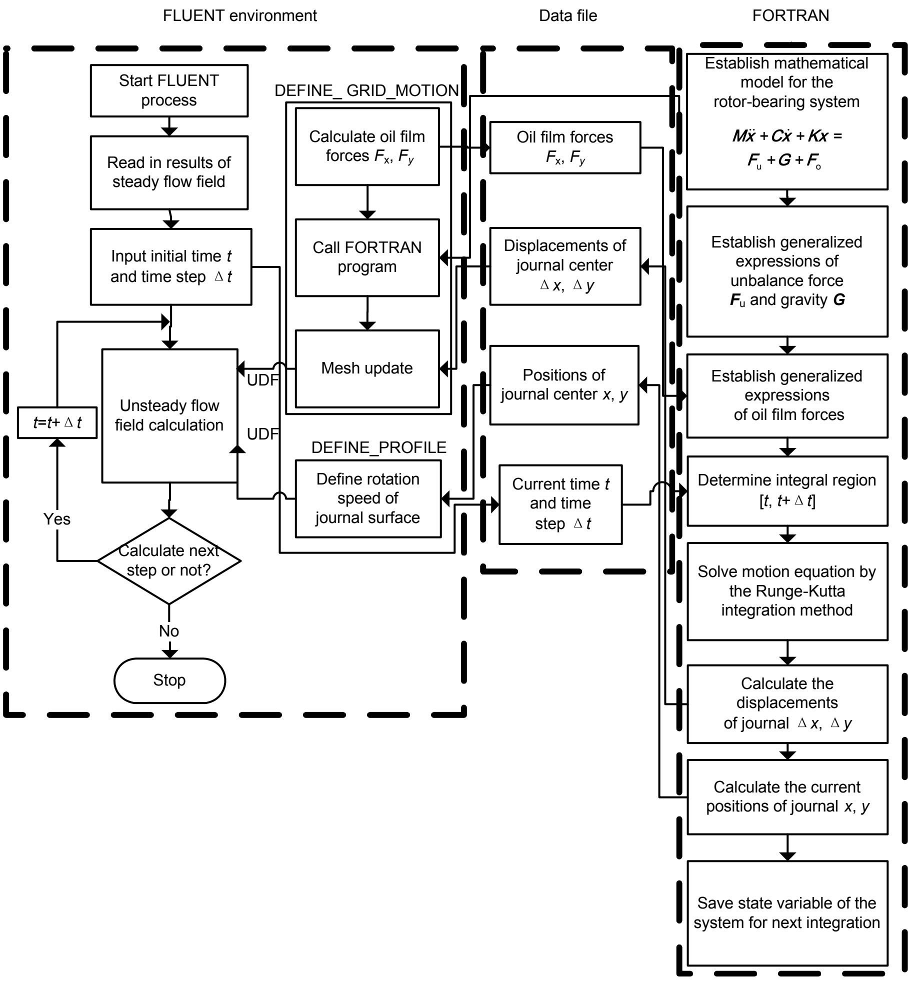

Fig. 5 FSI chart of the misaligned journal bearing analysis

solving the motion equation Eq. (8), using the fourth order Runge-Kutta in FORTRAN. Owing to the oil film force and moment, the perturbation displacement changes along the z axis. After the solid boundary condition is transferred to the data file, the CFD code is then applied to calculate the locus of the journal centre with the journal motion as prescribed boundary conditions, and update the grid position based on the proposed mesh movement method. This iterative procedure is repeated until the axis position is stable. Because the locus of the journal centre is changing with time during transient calculation, the rotational speed of the journal cannot be set by traditional methods. The second UDF using the DEFINE macro DEFINE_PROFILE is used to read the coordinates of the journal grids which change according to the instantaneous position of the journal. The tangential velocity in the surface of the journal is divided into two component velocities according to the new coordinate. The two component velocities plus the translational velocity component are given to the surface nodes of the journal by the macro DEFINE_PROFILE.

3.3 CFD model analysis

To prove that the CFD model can be applied to fluid film bearing analysis with necessary accuracy, a comparative study was conducted between the CFD solution and standard codes. The geometrical and operational data of the CFD model and the results of the standard codes from Guo *et al*. (2005) were used. The solutions of these three standard codes are based on the Reynolds equation, while FLUENT solves the general Navier-Stokes equations. Tables 1 and 2 give the results of static and dynamic calculations by FLUENT and by standard lubrication codes. Most of the static performance results and dynamic coefficients from FLUENT show a reasonable agreement with those from the standard codes. The signs of the cross stiffness and damping coefficients are opposite to those found by Guo *et al*. (2005) but the same as those found by Lund (1979).

Theoretically speaking, there are several simplifications associated with the classic Reynolds equation which is a reduced form of the Navier-Stokes equations and the continuity equation. Differences in the bases of the equations may explain the discrepancies found between the results of the static and dynamic analyses.

Firstly, in conventional lubrication, the inertia terms in the Navier-Stokes equations are negligible compared to the viscous terms. The effects of the fluid inertia on the journal orbits and static equilibrium position under different unbalance eccentricities and rotational speeds are shown in Figs. 6 and 7, respectively. The effects of the inertia terms are minimized by setting the density of the lubricant to a negligibly small value (1×10^{-10} kg/m^3). The radius of the whirling orbit with the inertia effect is smaller than that without the inertia effect, and the fluid inertia also has a significant effect on the static equilibrium position. So inertia effects must be dealt with carefully and included in the analyses, especially in transient condition. Although the traditional analysis can also take the inertia terms into account by modifying the Reynolds equation, more work is required to solve problems of greater complexity. Therefore, it would

Table 1 Results of static calculation

	Maximum pressure, p_{max} (MPa)	Relative deviation for p_{max} (%)	Oil film force, F (N)	Relative deviation for F (%)
VT-FAST	–	–	1151	3.015
DyRoBeS-BePerf	2.328	0.779	1155	2.678
VT-EXPRESS	2.336	1.125	1143	3.689
FLUENT	2.310	Reference	1186.78	Reference

Table 2 Stiffness and damping coefficients

	K_{xx} ($\times10^6$ N/m)	K_{xy} ($\times10^6$ N/m)	K_{yx} ($\times10^6$ N/m)	K_{yy} ($\times10^6$ N/m)	C_{xx} ($\times10^4$ N·s/m)	C_{xy} ($\times10^4$ N·s/m)	C_{yx} ($\times10^4$ N·s/m)	C_{yy} ($\times10^4$ N·s/m)
VT-FAST	40.0	−19.4	87.2	59.1	5.75	4.93	5.41	16.70
DyRoBeS-BePerf	38.0	−15.2	84.8	65.2	4.86	4.29	4.29	16.10
VT-EXPRESS	33.9	−13.1	85.3	65.0	4.38	3.87	4.50	15.90
FLUENT	43.4	22.4	−83.3	49.2	6.22	−5.82	−5.85	15.17

be very beneficial to use the CFD model in the field of hydrodynamic lubrication.

The second difficulty with the Reynolds equations is that it is 2D. Fig. 8 shows the pressure gradient in three directions of a journal bearing. The radial pressure gradient, which is neglected in standard lubrication solutions, is not small compared to the two other directions. In addition to the axial and tangential flows, radial flow exists due to the radial pressure gradient. Thus, a CFD model which takes into account 3D effects is needed.

The simulation based on the CFD model requires a great deal of calculation time, compared to the traditional analysis based on the Reynolds equation. This proves the efficiency of the standard lubrication solutions. The purpose of applying a general CFD code for hydrodynamic lubrication is not to replace the current standard lubrication solutions. Rather, it is necessary to understand the benefits of the CFD model in situations where a new complicated structure is used or where a more detailed analysis is necessary (Guo *et al*., 2005).

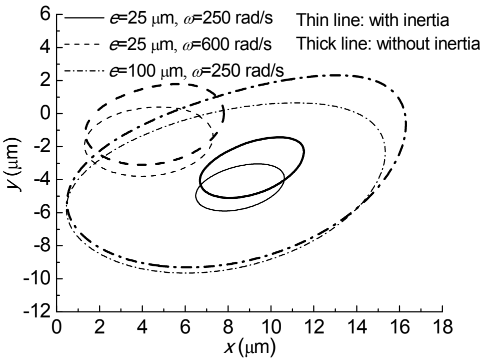

Fig. 6 Effect of fluid inertia on whirling orbits

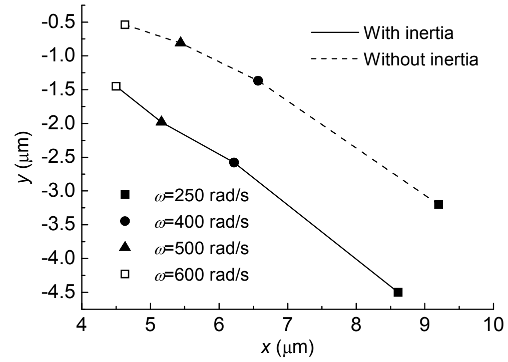

Fig. 7 Effect of fluid inertia on the static equilibrium position

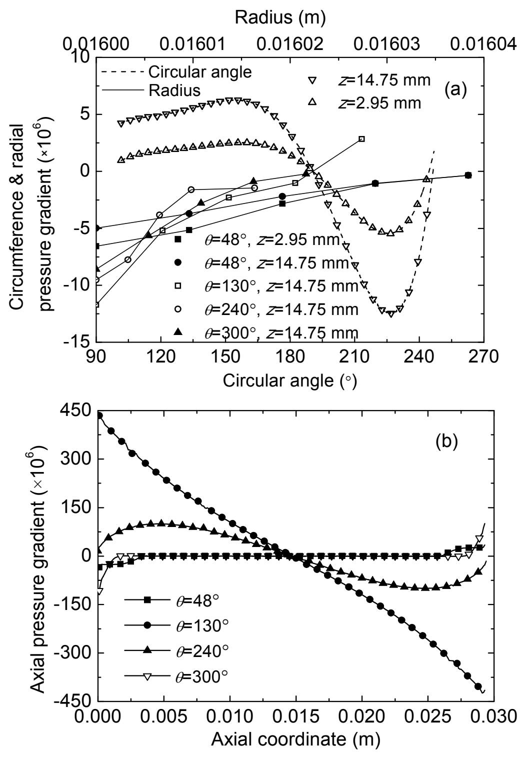

Fig. 8 Comparison of pressure gradient for circumference and radial directions (a) and axial direction (b)

4 Results and discussion

4.1 Model description

The rotor-bearing system used in this study is shown in Fig. 9. A flexible shaft with three disks is supported by two journal bearings. The left bearing is assumed to be a classical linearized bearing, and the load of the right journal bearing is nonlinear oil film force. Based on this system, a 3D model of the double groove journal bearing was built as shown in Fig. 10. Fig. 11 shows the configuration of a misaligned journal bearing. The severity of misalignment has been represented by two parameters, λ and γ, following Tieu *et al*. (1996). The misalignment ratio, λ, is defined as $\overline{O_oO_L}/(2c)$, and γ is the misalignment angle to the load direction at the mid-plane. The corresponding parameters of the shaft and journal bearing, operation condition and lubricant properties are given in Table 3.

The commercial packages GAMBIT and FLUENT are used as the grid generator and the CFD solver, respectively. Due to the difference in magnitude between the clearance size and the dimensions

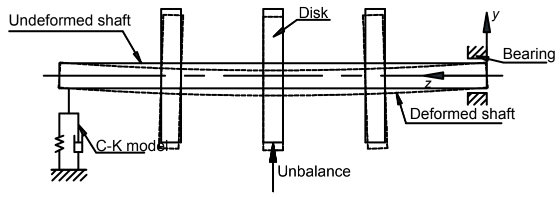

Fig. 9 A schematic diagram of the rotor-bearing system

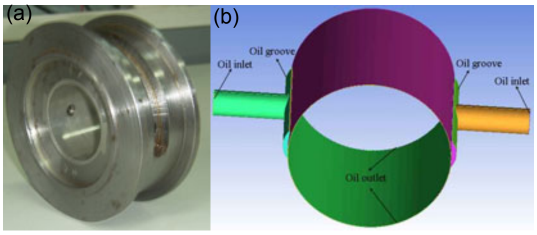

Fig. 10 Schematic of the journal bearing
(a) Practical model; (b) CFD model

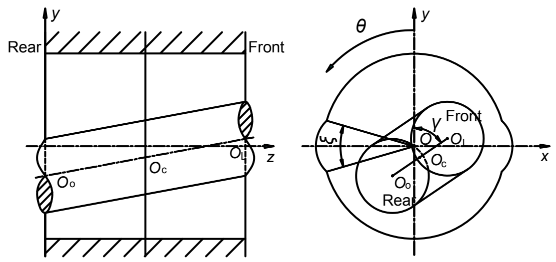

Fig. 11 Misaligned journal bearing

Table 3 Characteristics of the shaft and journal bearing, operating conditions and lubricant characteristics

Parameter	Value
Bearing width, l (mm)	29.5
Bearing radius, R (mm)	16
Radial clearance, c (mm)	0.032
Length of supply groove, L_g (mm)	14
Angular magnitude of supply groove, ξ (°)	25
Shaft length, L_s (mm)	1000
Disk mass, m_d (kg)	26.6
Disk radius, R_d (mm)	200
Elastic modulus of shaft, E (Pa)	2.06×10^{11}
Density of shaft, ρ_s (kg/m^3)	7800
Poisson's ratio, ν	0.3
Unbalance eccentricity, e (μm)	25–150
Unbalance phase, Φ_0 (°)	20
Rotational speed of bearing, ω (rad/s)	250–1000
Lubricant inlet pressure, p_i (Pa)	302 014.8
Ambient pressure, p_a (Pa)	101 325
Liquid saturation vapor pressure, p_{sat} (Pa)	29 185
Mass density of lubricant, ρ_l (kg/m^3)	850
Dynamic viscosity of lubricant, μ_l (Pa·s)	0.02

of the bearing, all applied meshes here are made using hexahedral cells in a regular structured mesh. Mesh aspect ratio influences the quality of the results and it is usually chosen as a value below 2 (Meruane and Pascual, 2008). Due to the existence of the thin film in journal bearings, previous work shows that it is possible to handle a large aspect ratio of a grid for bearing CFD models (Keogh *et al.*, 1997), because flows change very slowly in the circumferential and axial directions.

Simple boundary conditions are used for the oil inlet (pressure inlet), oil outlet (pressure outlet), moving journal (wall) and stationary bearing (wall) applied at the pre-processing stage (Gambit). At the boundary of the inlet, the lubricating oil flows into the journal bearing from the oil inlet in two grooves, and an appropriate pressure value leading to lubricant flow velocity is prescribed. At the boundary of the outlet, oil flows out from both sides with ambient pressure. On the surface of the bearing, a stationary wall condition is prescribed. The journal is modelled as a moving wall with an absolute rotational speed which is defined by a UDF program. The proposed mesh movement method associated with FLUENT is used for the transient flow due to the change of domain boundaries.

In the CFD multiphase simulation, the Navier-Stokes equations are solved in unsteady-state by the finite volume method. Since cavitation generally occurs when the pressure drops below the vapor pressure, the mixture model in FLUENT is used with a cavitation model. The phase coupled pressure-linked equations consistent (SIMPLEC) algorithm, which is an extension of the SIMPLEC algorithm to multiphase flows, is used for the pressure-velocity coupling. The first order upwind discretization scheme is used for the convection terms of each governing equation, except that the pressure is solved using the PRESTO (pressure staggering option) scheme. The iterative calculation starts with a preliminary, user-preset pressure field and the determination of the associated velocity field. Then, the pressure and velocity field are improved by means of a pressure correction equation giving interim solutions for all conservation equations. This iterative procedure is repeated until the equations meet the convergence criteria.

4.2 Grid convergence

The maximum pressure and load capacity are compared at a given eccentricity of ε=0.5 and ω= 1000 rad/s when three different mesh systems are applied. The first mesh density case uses 3, 105 and 340 divisions in the radial, axial and circumferential directions, respectively. For the second and third cases, the grid density is increased by factors of 1.5 and 3, respectively, in all direction. Results are given in Table 4 with respect to the situation with the highest density mesh. The difference in results for the maximum pressure and load capacity from the three different meshes is not large. To balance the calculation accuracy and the requirements for proper use of the machine's memory and simulation time, the Mesh 2 density (mesh aspect ratio of 42) is employed for the rest of this study.

4.3 Total time to steady-state convergence

For any given unbalance eccentricity excitation, during the whirling motion of the rotor, the pressure field reaches quasi-steady-state values. This means that the magnitude of the pressure field changes synchronously with the orbit after a short transient time. The time required to reach the steady synchronous rotation, and the appropriate computation time step size, are determined by means of a trial procedure during the numerical calculations (Xing *et al*., 2009).

The proof is shown in Table 5 where the confirmation of the time step size is indicated by the convergence in the maximum pressure and oil film force. The deviation for both maximum pressure and oil film force is below 0.7% when Δt=2×10^{-5} s, and thus all the calculations in this study are based on this time step size.

Based on this time step size, the total time to steady-state convergence is selected after a sensitivity analysis of the maximum pressure and oil film force, and the results are given in Table 6. The discrepancy in the calculated forces becomes relatively small after 6081 steps and becomes less than 0.6% after 8537 time steps. Thus, it can be concluded that the computation reached the steady-state operation for this unbalance eccentricity excitation after 8537 steps.

4.4 Validation of CFD model

Tieu and Qiu (1996) performed experiments on a misaligned journal bearing, and showed the pressure profile in the different axial positions. To validate the

Table 4 Grid convergence for computation (ε=0.5 and ω=1000 rad/s)

	No. of grids	Maximum pressure, p_{max} (Pa)	Relative deviation for p_{max} (%)	Load capacity, F_d (N)	Relative deviation for F_d (%)
Mesh 1	188881	7162157	12.87	2875.11	12.17
Mesh 2	557608	8112510	1.30	3259.141	0.443
Mesh 3	1456344	8219960	Reference	3273.656	Reference

Table 5 Time step size convergence (e=25 μm and ω=250 rad/s)

Time step size (s)	Maximum pressure, p_{max} (Pa)	Relative deviation for p_{max} (%)	Oil film force, F (N)	Relative deviation for F (%)
8×10^{-5}	994532.2	1.677	455.374	1.144
4×10^{-5}	1001846	0.954	457.943	0.587
3×10^{-5}	1002967	0.844	458.779	0.405
2×10^{-5}	1005126	0.630	459.647	0.217
1×10^{-5}	1011500	Reference	460.646	Reference

Table 6 Time convergence for computations (Δt=2×10^{-5} s, e=25 μm and ω=250 rad/s)

Times (s) (No. of time steps)	Maximum pressure, p_{max} (Pa)	Relative deviation for p_{max} (%)	Oil film force, F (N)	Relative deviation for F (%)
0.1216 (6081)	975957.5	2.37	448.947	2.26
0.1461 (7309)	988666.1	1.10	455.273	0.90
0.1707 (8537)	1005126	0.54	459.647	0.068
0.1953 (9765)	1008437	0.88	459.721	0.08
0.2199 (10993)	999661	Reference	459.335	Reference

present CFD scheme, the geometrical and operational data of the experimental apparatus from Tieu *et al.* (1996) were used. The bearing diameter and bearing length were both 200 mm, so the L/D used was 1.0. The radial clearance was 0.1455 mm. The oil viscosity was 0.007195 Pa·s at 60 °C and the Sommerfeld number was 0.045 (for a rotational speed of 402 r/min). Fig. 12 demonstrates the comparison of the simulated results for the misaligned bearing with the experimental measurements of Tieu and Qiu (1996). Very good concordance between the results of the two studies was found.

Fig. 13 shows the response of the journal obtained from different initial positions using the CFD model. The trajectories with different initial positions approach the same static equilibrium position when no dynamic external forces act on the system, and the static equilibrium position is the same as that obtained from static calculation. In the case with an unbalance eccentricity of e=25 μm, the journal continues its motion in an elliptical orbital path about the static equilibrium position. These results indicate that the transient calculation method in this study is reasonable.

4.5 Numerical results

The numerical results are given for the journal bearing of a flexible rotor-bearing system with two-axial oil grooves when journal misalignment takes place in the bearing hole caused by unbalance excitation. A comparison between aligned and misaligned bearings at varying values of unbalance eccentricity and rotational speed was made. The influence of misalignment with changing unbalance eccentricity and rotational speed on the bearing performances is also discussed.

Fig. 14 represents the journal orbit at three different axial positions of a journal bearing from the initial position at the bearing centre to the equilibrium position when the journal speed is 250 rad/s and the unbalance eccentricity is 20 μm. In the initial position, the oil force is obtained by a static analysis. Due to the unbalanced excitation of rotor, the shaft and the sleeve of the journal bearing are not aligned in the operating condition. Therefore, the whirl orbit of the axis at different positions along the axial direction of the journal bearing is different (Fig. 14), forming a conical orbit. The journal motion is initiated at the origin with forced and free vibrations. The free vibration decays rapidly due to oil film damping, and the journal centre spirals inward to its stable equilibrium position. In the final equilibrium position, the axis orbit is elliptic due to the unbalance of the rotor which is the main exciting source of the rotating machinery.

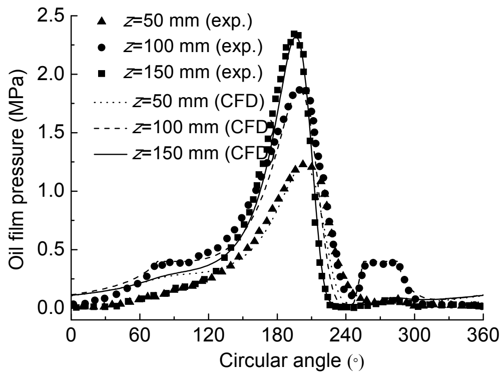

Fig. 12 Comparison of pressure distribution for the CFD model and experimental data by Tieu and Qiu (1996)

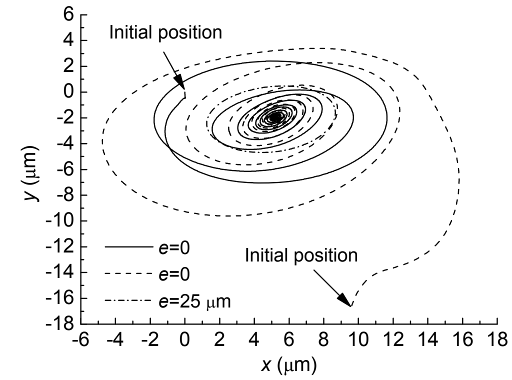

Fig. 13 Journal whirling orbits for different initial positions (ω=500 rad/s)

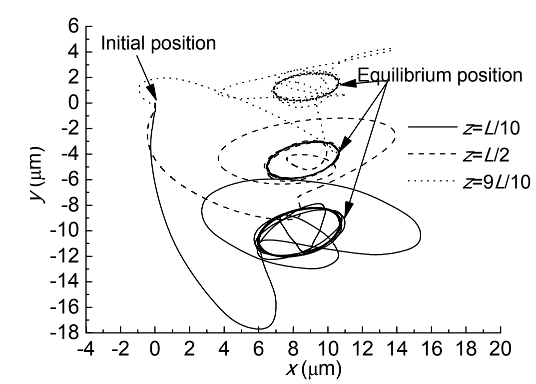

Fig. 14 Transient motion of axis (ω=250 rad/s and e=20 μm)

Fig. 15 shows 3D pressure distributions in journals with aligned or misaligned journal bearings, and Fig. 16 shows the corresponding cross-sections of the pressure distribution at the value of z ($z=L/10$). The comparison condition is that the unbalance eccentricity and rotational speed acting on the misaligned journal bearing are the same as those on the aligned journal bearing. The distribution of film pressure in the misaligned journal bearing is different from that in the aligned journal bearing. The highest film pressure is in the centre of length in the aligned journal bearing. However, in the misaligned journal bearing the highest film pressure moves to the end plane, showing a marked increase in cross-sections close to the end plane. Cavitation may occur nearby the convergence zone (Figs. 15a, 15c and 16). The reason for the shifting and increasing maximum film pressure is that the distribution of the film thickness changes due to the misalignment.

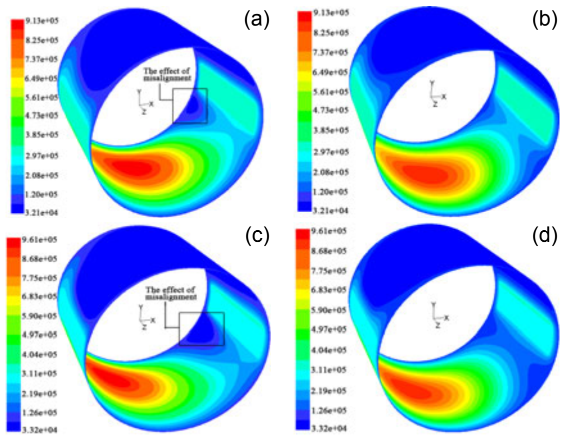

Fig. 15 Distribution of film pressure (Pa) in misaligned and aligned journal bearings

(a) λ=0.17, γ=14.17°, ω=250 rad/s, e=50 μm; (b) λ=0, γ=0, ω=250 rad/s, e=50 μm; (c) λ=0.17, γ=15.28°, ω=500 rad/s, e=25 μm; (d) λ=0, γ=0, ω=500 rad/s, e=25 μm

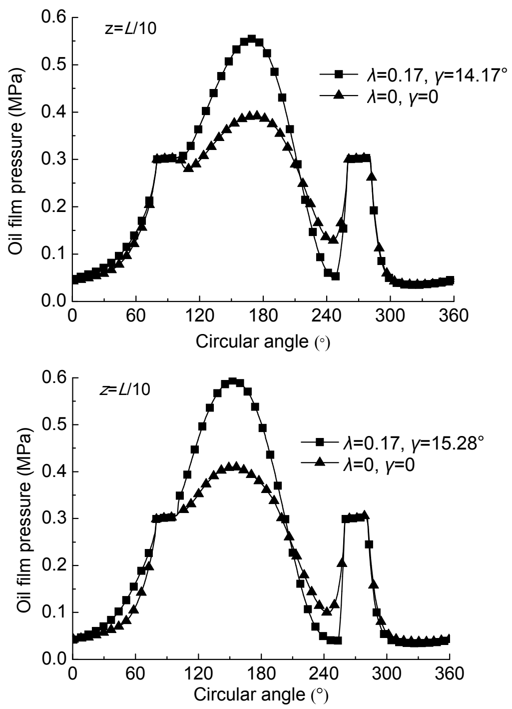

Fig. 16 Comparison of pressure distributions in misaligned and aligned journal bearings

(a) ω=250 rad/s, e=50 μm; (b) ω=500 rad/s, e=25 μm

Fig. 17 shows the variation in the ratio and angle of misalignment at different rotational speeds and unbalance eccentricities. The ratio and angle of misalignment increase with increasing unbalance eccentricity and rotational speed. But at speeds above a critical speed, the degree of misalignment decreases as rotational speed increases.

Fig. 18 represents the steady-state synchronous orbits obtained from various values of unbalance eccentricity ranging from 25 to 150 μm for the system corresponding to Fig. 9. The orbits obtained for the low unbalance values are nearly elliptical in shape. These trajectories and the resulting force can be closely approximated by the linear theory. As the unbalance eccentricity increases, the orbits depart from the elliptical shape, and the centre of the orbit is not at the steady-state balanced equilibrium position. In this case the linear bearing theory cannot be used to calculate the rotor orbit and the oil film force accurately. In the axial direction of bearing, the journal orbits of the aligned journal bearing are the same but those of the misaligned journal bearing are different.

Fig. 19 shows the steady-state synchronous orbits obtained for various speed values ranging from 250 to 1000 rad/s. Below the critical speed, the trajectory of the journal grows with increasing radii and a rising centre when the speed increases. Due to the nonlinear characteristics of the bearing, an increase in rotor speed can actually result in smaller amplitudes of motion and force when operating above the critical speed, but the whirling centre floats upward with the increasing speed. As the speed is further increased, the system loses its stability and the journal motion becomes chaotic. Clearly, the journal orbits of a misaligned journal bearing are different in the axial direction of bearing.

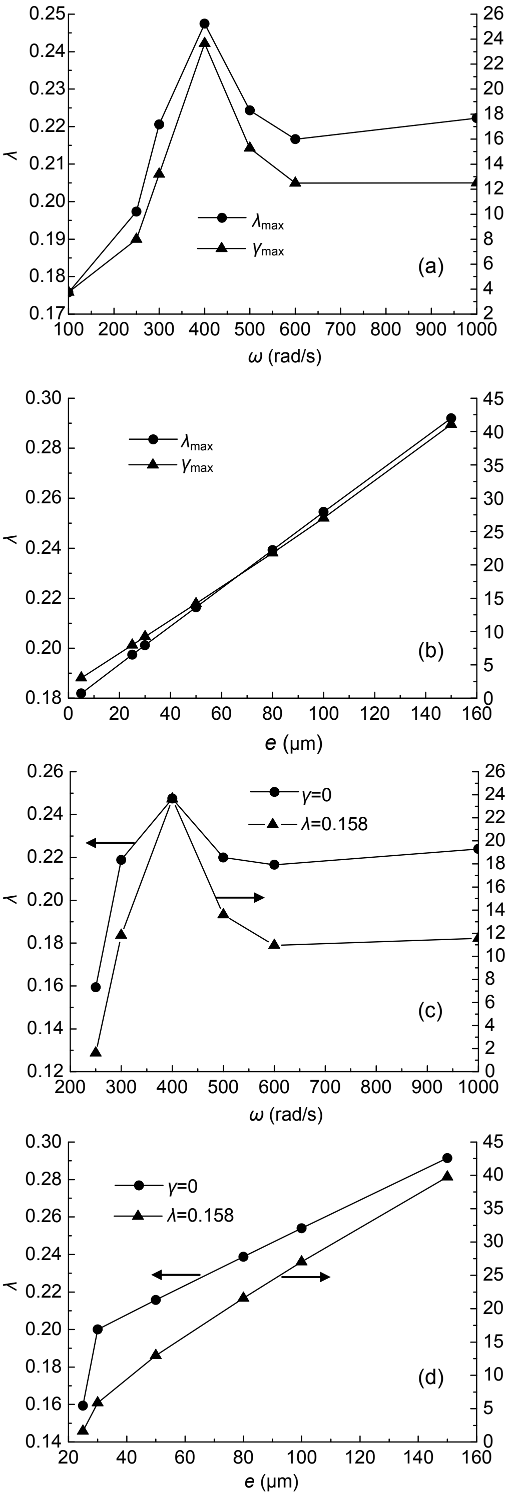

Fig. 17 Dependence of misalignment ratio and angle on speed (a) and (c), and unbalance eccentricity (b) and (d)

The values and locations of maximum pressure, misalignment moment M, oil film force F, friction torque M_τ, and attitude angle ψ of a journal bearing under different misalignment conditions due to various values of unbalance eccentricity and rotational speed are shown in Figs. 20 and 21. There are obvious offsetting distributions of film pressure and increases in the highest film pressure when journal misalignment takes place. When the degree of misalignment is small, the performance parameters do not vary appreciably compared to aligned bearing results. However, at higher degrees of misalignment, the maximum pressure and friction torque increase significantly beyond the aligned bearing values. The more the ratio is misaligned, the more obviously the maximum pressure, friction torque and misalignment moment increase. The oil film force also increases with the misalignment, but at a much lower rate than the maximum pressure. The misalignment effect on the attitude angle is small. The performance of a journal bearing also relates to the orientation of journal misalignment in the bearing, but γ has little influence on performance of a journal bearing (Figs. 20a and 20b). The influence of misalignment is reflected mainly by the misalignment ratio λ.

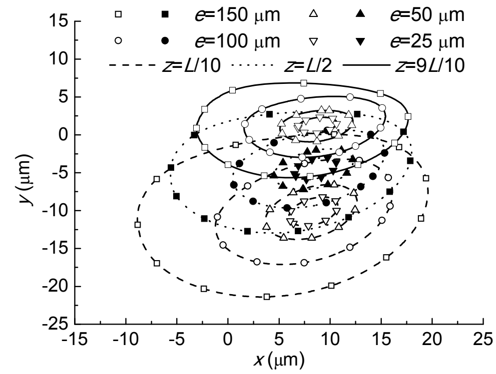

Fig. 18 Journal orbits under different unbalance eccentricities

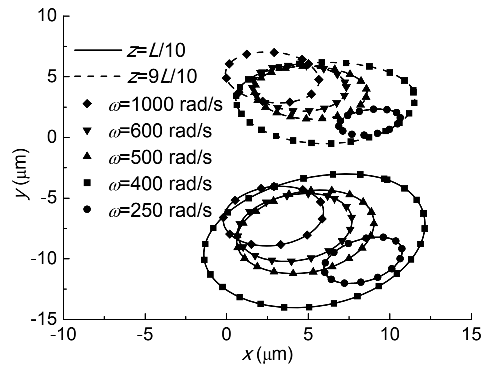

Fig. 19 Journal orbits under different rotational speeds

5 Conclusions

A new numerical analysis of the effects of misalignment on the transient flow field of a double-grooved journal bearing in a flexible rotor-bearing system is proposed in this paper. CFD and FSI methodologies are used in this analysis. Both inertial and cavitational effects are considered. The results of a CFD model are found to be in very good agreement with previous experimental results (Tieu and Qiu, 1996). The following conclusions can be made:

1. Compared with three existing dynamic mesh methods in FLUENT, the proposed mesh movement method can achieve optimal grid quality of the displaced grid at any time step. It can also provide a basis for modeling the transient simulation under arbitrary journal disturbance.

2. The new CFD method based on a fluid-structure coupling method is used to calculate the transient fluid dynamics of the oil film in journal bearing and rotor dynamics. It is shown to be a useful tool for the investigation of the effects of misalignment

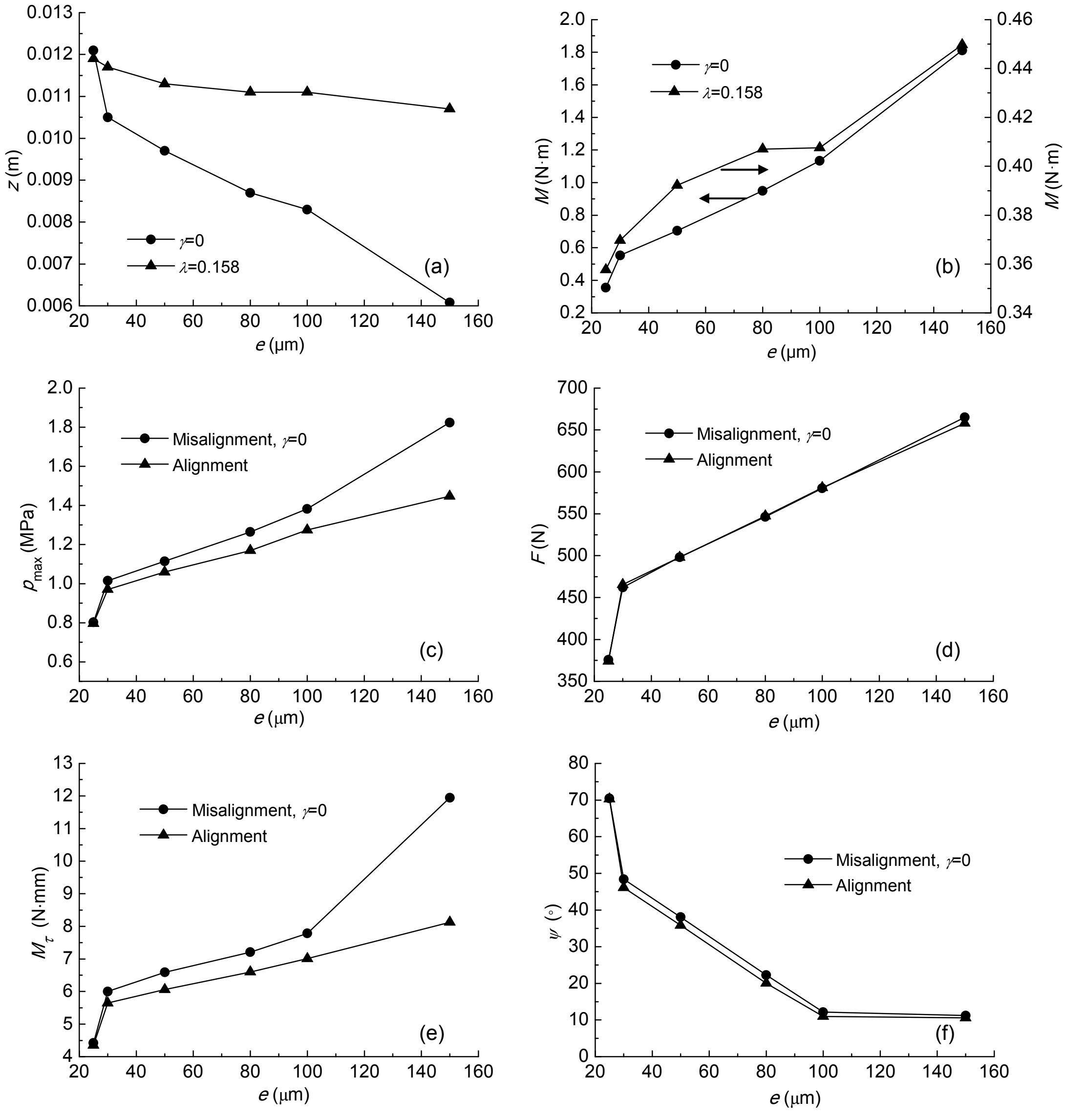

Fig. 20 Effects of misalignment due to unbalance eccentricity on the performance of a journal bearing
(a) Position of maximum pressure; (b) Misalignment moment; (c) Maximum pressure; (d) Oil film force; (e) Friction torque; (f) Attitude angle

on the transient flow field and performance characteristics of journal bearings. The locus of the journal center considering misalignment caused by unbalanced rotor mass can be determined accurately by this method.

3. The effects of journal misalignment on the hydrodynamic performance of a double-grooved bearing were analyzed. There were obvious changes in film pressure distribution and maximum film pressure when the journal was misaligned. The location of the highest film pressure moved to the end of the bearing as the degree of misalignment increased. The values of maximum film pressure, friction torque, and misalignment moment increased markedly when the degree of misalignment increased. However, the oil film force and attitude angle did not vary significantly with the misalignment. Thus, journal misalignment in the bearing hole should be included in calculating the performance characteristics of a journal bearing.

References

Arumugam, P., Swarnamani, S., Prabhu, B.S., 1997. Effects of journal misalignment on the performance characteristics of three-lobe bearings. *Wear*, **206**(1-2):122-129. [doi:10.1016/S0043-1648(96)07337-1]

Asanable, S., Akahoshi, M., Asai, R., 1971. Theoretical and

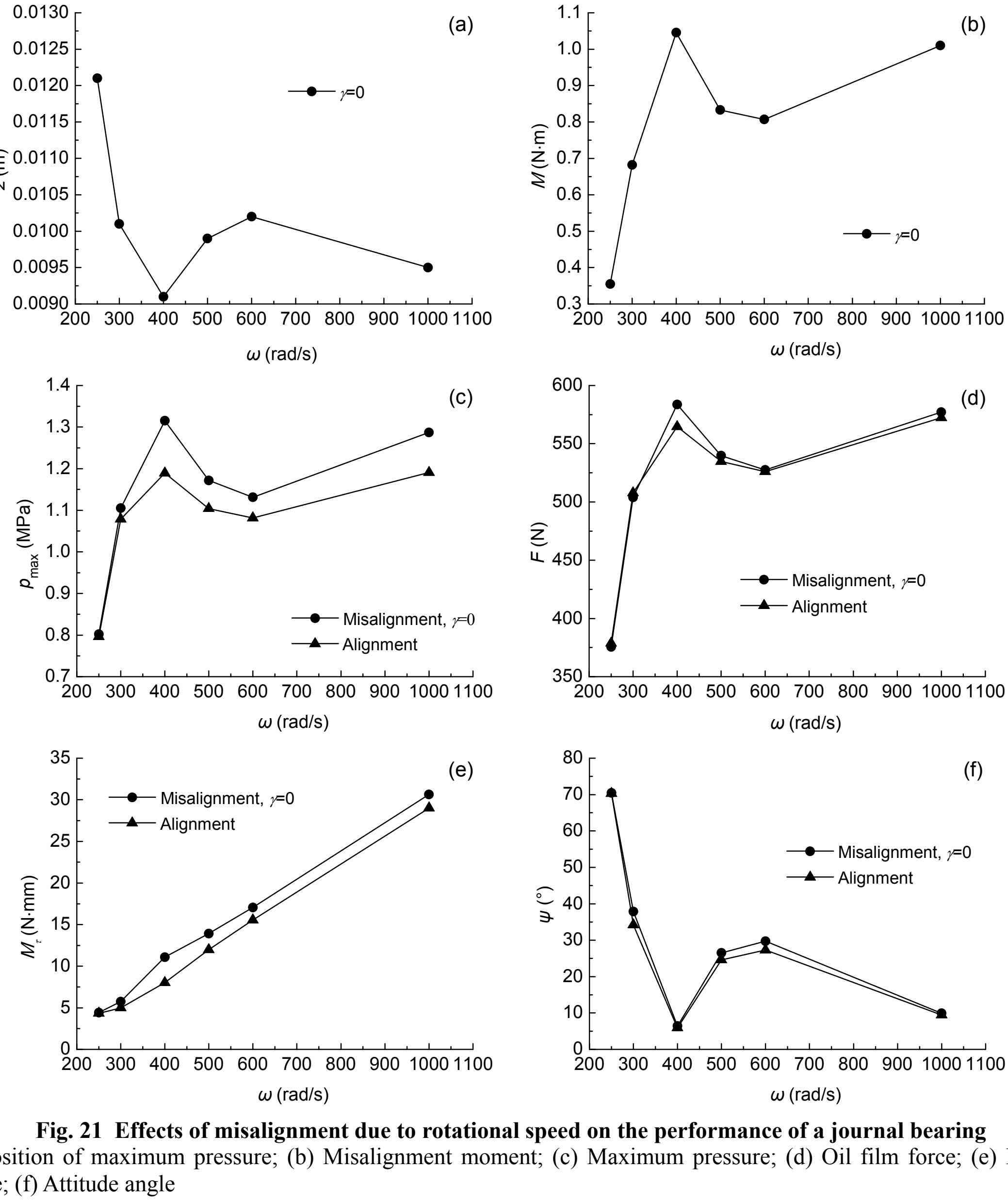

Fig. 21 Effects of misalignment due to rotational speed on the performance of a journal bearing
(a) Position of maximum pressure; (b) Misalignment moment; (c) Maximum pressure; (d) Oil film force; (e) Friction torque; (f) Attitude angle

Experimental Investigation of Misaligned Journal Bearing Performance. Tribology Convention, Institution of Mechanical Engineers, London, C36/71.

Banwait, S.S., Chandrawat, H.N., Adithan, M., 1998. Thermohydrodynamic Analysis of Misaligned Plain Journal Bearing. Proceeding of First Asia International Conference on Tribology, Beijing, p.35-40.

Boedo, S., Booker, J.F., 2004. Classic bearing misalignment and edge loading: a numerical study of limiting cases. *Journal of Tribology*, **126**(3):535-541. [doi:10.1115/1.1739241]

Bouyer, J., Fillon, M., 2002. An experimental analysis of misalignment effects on hydrodynamic plain journal bearing performances. *Journal of Tribology*, **124**(2):313-319. [doi:10.1115/1.1402180]

Bou-Said, B., Nicolas, D., 1992. Effects of misalignment on static and dynamic characteristics of hybrid bearings. *Tribology Transactions*, **35**(2):325-331.

Buckholz, R.H., Lin, J.F., 1986. The effect of journal bearing misalignment on load and cavitation for non-Newton lubricants. *Journal of Tribology*, **108**(4):645-654. [doi:10.1115/1.3261295]

Chen, P.Y.P., Hahn, E.J., 1998. Use of computational fluid dynamics in hydrodynamic lubrication. *Journal of Engineering Tribology*, **212**(6):427-436. [doi:10.1243/1350650981542236]

Chen, P.Y.P., Hahn, E.J., 2000. Side clearance effects on squeeze film damper performance. *Tribology International*, **33**(3-4):161-165. [doi:10.1016/S0301-679X(00)00022-0]

Dowson, D., Taylor, C.M., 1979. Cavitation in bearings. *Annual Review of Fluid Mechanics*, **11**(1):35-66. [doi:10.1146/annurev.fl.11.010179.000343]

Dubois, G.B., Ocvirk, F.W., Wehe, R.L., 1951. Experimental Investigation of Oil Film Pressure Distribution for Misaligned Plain Bearings. NCAC, Technical Note 2507, Washington.

Dubois, G.B., Mabic, H.H., Ocvirk, F.W., 1955. Experimental Investigation of Misalignment Couples and Eccentricity at Ends of Misaligned Plain Bearings. NCAC, Technical Note 3352, Washington.

Dubois, G.B., Ocvirk, F.W., Wehe, R.L., 1957. Properties of misaligned journal bearing. *Journal of Basic Engineering*, **79**:1205-1212.

FLUENT, 2006. Fluent 6.3 User's Guide. New Hampshire (USA) Fluent Incorporation, Lebanon.

Gertzos, K.P., Nikolakopoulos, P.G., Papadopoulos, C.A., 2008. CFD analysis of journal bearing hydrodynamic lubrication by Bingham lubricant. *Tribology International*, **41**(12):1190-1204. [doi:10.1016/j.triboint.2008.03.002]

Guha, S.K., 2000. Analysis of steady-state characteristics of misaligned hydrodynamic journal bearings with isotropic roughness effect. *Tribology International*, **33**(1):1-12. [doi:10.1016/S0301-679X(00)00005-0]

Guo, Z.L., Hirano, T., Kirk, R.G., 2005. Application of CFD analysis for rotating machinery. part I. hydrodynamic, hydrostatic bearings and squeeze film damper. *Journal of Engineering for Gas Turbines and Power*, **127**(2):445-451. [doi:10.1115/1.1807415]

Jakobsson, B., Floberg, L., 1957. The Finite Journal Bearing Considering Vaporization. Chalmers Tekniska Hoegskolas Handlingar, **190**:28-101.

Jang, J.Y., Chang, C.C., 1987. Adiabatic solution for a misaligned journal bearing with non-Newtonian lubricants. *Tribology International*, **20**(5):267-275. [doi:10.1016/0301-679X(87)90027-2]

Jang, J.Y., Khonsari, M.M., 2010. On the behavior of misaligned journal bearings based on mass-conservative thermohydrodynamic analysis. *Journal of Tribology*, **132**(1):011702. [doi:10.1115/1.4000280]

Keogh, P.S., Gomiciaga, R., Khonsari, M.M., 1997. CFD based design techniques for thermal prediction in a generic two-axial groove hydrodynamic journal bearing. *Journal of Tribology*, **119**(3):428-435. [doi:10.1115/1.2833511]

Li, W., Yang, Y., Sheng, D.R., Chen, J.H., Che, Y.Q., 2011. Nonlinear dynamic analysis of a rotor/bearing/seal system. *Journal of Zhejiang University-SCIENCE A (Applied Physics & Engineering)*, **12**(1):46-55. [doi:10.1631/jzus.A1000130]

Liu, H.P., Xu, H., Ellison, P.J., Jin, Z.M., 2010. Application of computational fluid dynamics and fluid-structure interaction method to the lubrication study of a rotor-bearing system. *Tribology Letters*, **38**(3):325-336. [doi:10.1007/s11249-010-9612-6]

Lund, J.W., 1979. Rotor-Bearing Dynamics, Lecture Notes, Technical University of Denmark, Denmark.

Ma, Y.Y., 2008. Performance of dynamically loaded journal bearings lubricated with couple stress fluids considering the elasticity of the liner. *Journal of Zhejiang University-SCIENCE A (Applied Physics & Engineering)*, **9**(7):916-921. [doi:10.1631/jzus.A0720085]

McKee, S.A., McKee, T.R., 1932. Pressure distribution in the oil film of journal bearings. *Transactions of the ASME*, **54**:149-165.

Meruane, V., Pascual, R., 2008. Identification of nonlinear dynamic coefficients in plain journal bearings. *Tribology International*, **41**(8):743-754. [doi:10.1016/j.triboint.2008.01.002]

Mokhtar, M.O.A., Safar, Z.S., Abd-EI-Rahman, M.A.M., 1985. An adiabatic solution of misalignment journal bearings. *ASME Journal of Lubrication Technology*, **107**(2):263-267. [doi:10.1115/1.3261041]

Ngondi, E.M., Grönsfelder, T., Nordmann, R., 2010. Mesh movement method for transient simulation of annular cavities: application to prediction of fluid forces in squeeze film dampers. *Tribology Transactions*, **53**(3):440-451. [doi:10.1080/10402000903420779]

Pierre, I., Bouyer, J., Fillon, M., 2004. Thermohydrodynamic behavior of misaligned plain journal bearings: theoretical and experimental approaches. *Tribology Transactions*, **47**(4):594-604. [doi:10.1080/05698190490513974]

Pinkus, O., Bupara, S.S., 1979. Analysis of misaligned grooved journal bearings. *Journal of Lubrication Tech-*

nology, **101**(4):503-509. [doi:10.1115/1.3453402]

Qiu, Z.L., Tieu, A.K., 1995. Misalignment effect on the static and dynamic characteristics of hydrodynamic journal bearings. *Journal of Tribology*, **117**(4):717-723. [doi:10.1115/1.2831542]

Qiu, Z.L., Tieu, A.K., 1996. Experimental study of freely alignable journal bearings-part 2: dynamic characteristics. *Journal of Tribology*, **118**(3):503-508. [doi:10.1115/1.2831566]

Singhal, A.K., Athavale, M.M., Li, H.Y., Jiang, Y., 2002. Mathematical basis and validation of the full cavitation model. *Journal of Fluids Engineering*, **124**(3):617-624. [doi:10.1115/1.1486223]

Smalley, A.J., McCallion, H., 1966. The Effect of Journal Misalignment on the Performance of a Journal Bearing Under Steady Running Conditions. Proceedings of Institution of Mechanical Engineers, **181**(Pt.3B):45-54. [doi:10.1243/PIME_CONF_1966_181_031_02]

Sun, J., Deng, M., Fu, Y.H., Gui, C.L., 2010. Thermohydrodynamic lubrication analysis of misaligned plain journal bearing with rough surface. *Journal of Tribology*, **132**(1):011704. [doi:10.1115/1.4000515]

Sun, J., Gui, C.L., 2004. Hydrodynamic lubrication analysis of journal bearing considering misalignment caused by shaft deformation. *Tribology International*, **37**(10):841-848. [doi:10.1016/j.triboint.2004.05.007]

Sun, J., Gui, C.L., Li, Z.Y., 2005. Influence of journal misalignment caused by shaft deformation under rotational load on performance of journal bearing. *Journal of Engineering Tribology*, **219**(4):275-283. [doi:10.1243/135065005X33937]

Sun, J., Gui, C.L., Wang, J.F., 2007. Research on shaft strength considering offsetting distribution of film pressure of journal bearing in shaft-bearing system. *Journal of Mechanical Engineering Science*, **221**(1):99-107. [doi:10.1243/0954406JMES352]

Tieu, A.K., Qiu, Z.L., 1996. Experimental study of freely alignable journal bearings-part 1: static characteristics. *ASME Journal of Tribology*, **118**(3):498-502. [doi:10.1115/1.2831565]

Vijayaraghavan, D., Keith, T.G., 1989. Effect of cavitation on the performance of a grooved misaligned journal bearing. *Wear*, **134**(2):377-397. [doi:10.1016/0043-1648(89)90137-3]

Vijayaraghavan, D., Keith, T.G., 1990. Analysis of a finite misaligned journal bearing considering cavitation and starvation effects. *Journal of Tribology*, **112**(1):60-67. [doi:10.1115/1.2920231]

Xing, C.G., Braun, M.J., Li, H.M., 2009. A three-dimensional Navier-Stokes-Based numerical model for squeeze-film dampers. Part 1-effects of gaseous cavitation on pressure distribution and damping coefficients without considering of inertia. *Tribology Transactions*, **52**(5):680-694. [doi:10.1080/10402000902913303]

Zheng, S.Y., 1993. Lernende Regelung Für Rotorsysteme. Fortschritt-Berichte VDI, VDI-Verlag, Duesseldorf, Germany, p.1-24 (in German).

Zheng, S.Y., Liu, S.L., 2005. On-line elimination of oil whip. *Chinese Journal of Mechanical Engineering*, **18**(2):228-231. [doi:10.3901/CJME.2005.02.228]

Recommended reading

Zhang, H.J., Zhu, C.S., Yang, Q., 2009. New numerical solution for self-acting gas journal bearings. *Journal of Zhejiang University-SCIENCE A (Applied Physics & Engineering)*, **10**(5):685-690. [doi:10.1631/jzus.A0820532]

Liu, H.P., Xu, H., Jin, Z.M., Ellison, P.J., 2010. Lubrication analysis of journal bearing and rotor system using CFD and FSI techniques. *Advanced Tribology*, **3**(1):40-41. [doi:10.1007/978-3-642-03653-8_15]

Xing, C.H., Braun, M.J., Li, H.M., 2010. Damping and added mass coefficients for a squeeze film damper using the full 3-D Navier-Stokes equation. *Tribology International*, **43**(3):654-666. [doi:10.1016/j.triboint.2009.10.005]

Li, W., Yang, Y., Sheng, D.R., Chen, J.H., Che, Y.Q., 2011. Nonlinear dynamic analysis of a rotor/bearing/seal system. *Journal of Zhejiang University-SCIENCE A (Applied Physics & Engineering)*, **12**(1):46-55. [doi:10.1631/jzus.A1000130]